Computer Modeling in
Engineering & Sciences

Tech Science Press

https://doi.org/10.32604/cmes.2026.083185

ARTICLE

High-Fidelity Co-Simulation Framework toward Digital Twin-Based Interturn Short-Circuit Fault Diagnosis in Interior Permanent Magnet Synchronous Motor

Junho Lee, Sanghyun Park, Younghun Lee and Namsu Kim*

Department of Mechanical Engineering, Konkuk University, Seoul, Republic of Korea

*Corresponding Author: Namsu Kim. Email: nkim7@konkuk.ac.kr

Received: 30 March 2026; Accepted: 18 May 2026; Published: 27 July 2026

ABSTRACT: Monitoring the conditions of electric motors in industrial applications is an essential step for ensuring safety and reducing maintenance costs. This paper deals with one of the most frequent winding failures—the interturn short fault of an interior permanent magnet synchronous motor. A novel high-fidelity co-simulation framework toward a digital twin-based approach combining Maxwell simulation in finite element method (FEM) for the motor and control system in system software for the inverter is presented. An analysis of the motor based on a 2D FEM model is performed considering the motor topology and non-linear properties, and inductance and flux-linkage data of 3-phase and short circuit currents. A real-time simulation of the motor and inverter control algorithm is performed based on the calculated electromagnetic field data of the motor. The characteristics of short current and its fault diagnosis method under different operating conditions, according to short fault severity, load, and speed of motor, are investigated. We focused on phase current spectral analysis, particularly the 3rd harmonics of the phase current in the frequency domain. The proposed co-simulation approach enables a digital twin-based model to identify and pick up informative data for fault diagnosis. In addition, the simulation results and proposed method are verified using experimental data.

KEYWORDS: Digital twin-based approach; co-simulation; interturn short-circuit fault; permanent magnet synchronous motor; fault detection

1 Introduction

The demand for electric vehicles (EVs) has continued to increase in order to replace internal combustion engine vehicles, owing to increasing environmental problems and the corresponding environmental regulations. In addition, electric motors are used in a vast range of industrial applications, from powering pumps, fans, compressors, lifts in manufacturing systems, and actuators in robots. An interior permanent magnet synchronous motor (IPMSM), frequently used as a traction motor for EVs as well as industrial applications, may fail owing to various mechanical and electrical faults such as bearing faults, eccentricity, demagnetization, and winding short; therefore, research on prognostic and health management (PHM) of IPMSM has been actively conducted [1].

Recent research investigated an 800 V electrified vehicle platform to ensure fast battery charging and high power [2–5]. Furthermore, construction vehicles, trucks, and high-performance vehicles have been manufactured based on an 800 V system [6,7]. However, when a high voltage is applied to the winding, the strength of the electric field may exceed the dielectric strength in the gap between the insulators inside the winding insulation or between the windings, causing partial discharge. The partial discharge causes a high-temperature electric spark to erode the insulator, and the ozone generated by the partial discharge causes a chemical reaction in the insulator, deteriorating the insulation performance [8,9]. Partial discharge continuously deteriorates the winding insulation, and eventually, the insulation fails, causing an interturn short-circuit fault (ITSF) in the winding of the motor. In addition, the high switching frequency characteristic of the wide band gap (WBG) power module for increasing the efficiency of the inverter also increases the number of occurrences of partial discharge [10]. Next-generation power modules for electric vehicles as well as industrial applications mainly adopt silicon carbide (SiC) and gallium nitride (GaN) based switching devices as they have a high slew rate of 50–100 kV/μs compared with 20 kV/μs for conventional switching devices and achieve high efficiency by reducing low-order harmonics and switching loss; however, such a high slew rate generates an inverter surge voltage (close to twice the applied voltage) and accelerates the partial discharge energy [3]. According to [11], stator winding failure can account for 36%–66% of the failure modes of the electric machine as the applied voltage increases.

In previous studies, winding fault diagnosis was mainly performed using various signals such as current, voltage, and magnetic flux sensors. Among these, motor current signature analysis (MCSA) has been studied using various signal processing techniques such as fast Fourier transform (FFT) [12], short-time Fourier transform (STFT) [13], and additional sensors to investigate current [14,15]. Unlike other failure diagnosis methods, MCSA can be performed using the current sensor embedded in the traction system of EVs without requiring additional sensors.

Urresty et al. [16] used the zero-sequence voltage component of the voltage between the three phases and the neutral point to diagnose ITSF. Sarikhani and Mohammed [17] used the back electromotive force (back EMF) of a faulty motor estimated based on the current and line voltage, and the failure was diagnosed by comparing the back EMF with that measured from a healthy motor. Other studies used the signal injection method at standstill conditions [18,19]. Qi et al. [18] used the high-frequency signal injection method to estimate the number of shorted turns by calculating the resistance and inductance of the winding. Baruti et al. [19] applied DC current to the stator winding and developed a severity estimation algorithm considering the non-linearity of inverter switching modules. Although these signal injection-based methods can be performed only at standstill conditions, they have a significant advantage in that they are not affected by the operating conditions, unlike other methods, and can maintain good fault diagnosis accuracy. Despite its advantages, this method is fundamentally limited by its inability to function while the motor is in motion.

A stator winding short-circuit fault can be classified into three types: ITSF, phase-to-phase short-circuit fault, and phase-to-ground short-circuit fault. ITSF refers to a short circuit fault in a single coil and is the most common short-circuit fault type [20,21] because coils are insulated only with the weakest enamel coating. When a short circuit occurs between turns, it causes a decrease in motor efficiency and vibration of the motor. In addition, a short circuit current exceeding the current capacity of the winding can be induced in the short region. Early detection of ITSF is necessary because short circuit current can cause excessive thermal stress on the windings, leading to catastrophic motor failure, i.e., phase-to-phase short-circuit fault, and phase-to-ground short-circuit fault.

Stator coils are randomly distributed within the slots, and a short-circuit fault can occur anywhere; therefore, the number of shorted turns is also unpredictable. The number of shorted turns is closely related to the amplitude of the short current [22–24] or circulating current that causes excessive heat [23,25,26] and flux distortion [27]. As the number of shorted turns increases, the short current decreases and then increases [22,23]; hence, the number of shorted turns and short current can be proportional or inversely proportional depending on the contact resistance [25,26]. According to the above studies, the relationship between the number of shorted turns and short current can change depending on motor parameters such as motor topology, power, and contact resistance; therefore, this relationship should be carefully investigated.

Recently, the paradigm of system fault diagnosis, including motor systems, has shifted toward a co-simulation or digital twin-based approach. These offer an enhanced and comprehensive understanding of physical degradation induced by motor faults, predictive capabilities, and design guidelines for diagnosis systems based on results from high-fidelity virtual models [20,28,29]. Despite these advancements, achieving a balance between model fidelity and computational efficiency remains a significant challenge. While full-scale Finite Element Method (FEM) models provide superior accuracy in capturing nonlinear electromagnetic behaviors during faults, their integration into real-time digital twin environments is often hindered by prohibitive computational costs [30]. To address these limitations, recent cutting-edge literature has explored Reduced-Order Modeling (ROM) and Look-up Table (LUT)-based co-simulations as a pragmatic path toward functional Digital Twins. By embedding control algorithms directly into the simulation loop, these approaches can replicate the phase current signatures that are critical for industrial diagnosis, which were often simplified in earlier studies.

This study proposes a novel high-fidelity co-simulation framework toward a digital twin-based approach for the diagnosis of ITSF of IPMSM. Finite element analysis (FEA) was performed to obtain the inductance and flux linkage data of the healthy condition and ITSF of the motor. A closed-loop controlled inverter–motor system was co-simulated using the inductance and flux linkage data to calculate the phase current. Specifically, the inverter modeling for motor control involved programming the control algorithm, and the simulation parameters were tuned to ensure that the resulting current values closely matched the experimental data. Our co-simulation model achieves significantly improved accuracy for calculating the phase current with an error of only 15% under identical conditions. Based on results from co-simulation, we demonstrated that ITSF can be diagnosed via frequency domain analysis and established the specific frequency range required for observation. In addition, the severity levels of diagnosable ITSF were identified. To verify the simulation results, faulty IPMSMs were designed and assembled with artificially emulated ITSF with different severity levels. The monitored data of the phase current, including short current as well as vibration, were analyzed under various operating conditions. Furthermore, it was confirmed that ITSF diagnosis can be effectively performed using low-cost, embedded current sensor data from the traction system, rather than relying on expensive vibration data. The main advantage of the proposed experimental set-up, including the system for prognostics and health management (PHM), is to control the severity level of shorts as well as the contact resistance of shorted points. This approach can provide guidelines for a maintenance schedule.

2 Co-Simulation of Inverter–Motor

Many analytical techniques can be used for modeling short-circuit faults of motors. Among them, finite element analysis (FEA)-based modeling is an accurate modeling technique as it considers the non-linear characteristics caused by magnetic saturation and the topology of the motor. In a couple of studies, an IPMSM control drive model coupled with FEA simulation was simulated [31,32]. Although this co-simulation method provides accurate analysis results, it requires significant simulation time. As a result, Qi et al. [26] used an FE-based phase variable model to analyze the FEA and control algorithm to reduce the computational time. In their study, FEA simulation was performed to create a look-up table (LUT) of inductance and flux linkage on each rotor position, and a 3-phase voltage drive model was simulated using the LUT. Once the FEA simulation has been performed, it is not necessary to perform it while simulating the drive model under various operating conditions. This method is frequently used for fault motor analysis because it yields relatively accurate analysis results in less time compared with the co-simulation method. Therefore, during the real-time co-simulation, the system instantly retrives there pre-computed values instead of solving complex, time-consuming electromagnetic equations at every time step.

2.1 Finite Element Analysis

In this study, a 2D FEA analysis was performed using the Ansys Maxwell program to evaluate the electromagnetic effect of an ITSF in the motor. A 400 W IPMSM with two pole pairs was modeled, and the non-linear magnetic properties of the material were considered. Fig. 1 shows a model of the IPMSM including its geometry and topology. The detailed specifications of the IPMSM are presented in Table 1. Fig. 2 shows the winding model of the IPMSM with ITSF. The winding model consists of three phases, with one phase comprising three coils with 42 turns; only one coil is shown for convenience. To examine the characteristics of the ITSF based on the number of shorted turns, three faults were implemented by connecting the neutral point, which is the middle point of the last coil of phase A, as shown in Fig. 2. The number of shorted turns is set by 1st, 13th, and 26th in the IPMSM. Phase A was divided into a healthy coil and a shorted coil. FEA simulation was performed for three types of ITSF. The flux linkage and inductance for three phases and short-circuited phases were calculated according to the rotor position in the range of 0°–360° electrical angle. The simulation was conducted on a workstation equipped with an Intel Xeon W-5 3435X CPU (16 cores, 32 threads, Max 4.5 GHz), 128 GB RAM, RTX A2000 12 GB GPU.

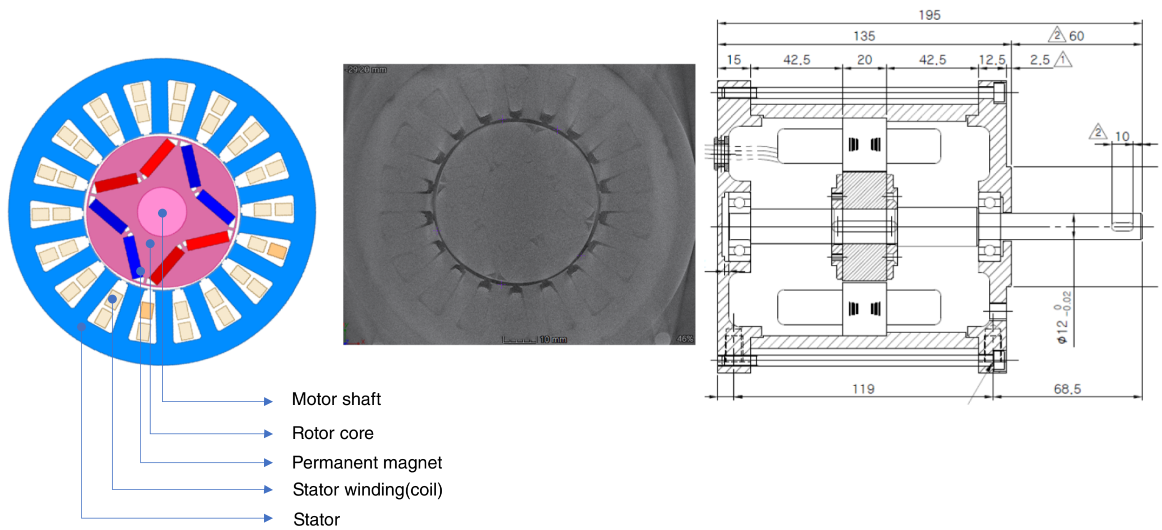

Figure 1: Geometry and topology of modeled IPMSM (left), Computed Tomography (CT) for topology, and detailed sectional view drawing (right) of motor used in both simulation and experiment.

Table 1: Detailed specification of the IPMSM used in this study.

Motor Parameters	Value
Motor type	IPMSM
Winding type	Double layer
Number of rotor poles	4
Rated power	0.4 kW
Rated torque	0.58 N·m
Rated speed	6600 rpm
Rated voltage	220 V
System inertia	44.4
Ld	6.68 mH

(Continued)

Table 1 (continued)

Motor Parameters	Value
Lq	13.39 mH
Resistance (phase)	1.139 Ω
λPM	0.1025 Wb

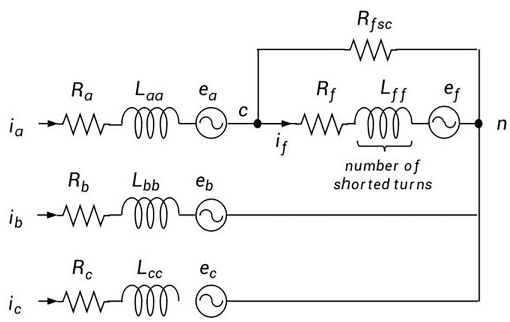

Figure 2: Winding configuration of the ITSF motor.

2.2 ITSF in IPMSM Modeling

The phase voltage model of the ITSF of IPMSM is represented by the following voltage, torque, and motion equations. As the motor voltage is applied as a line voltage, the equation is represented as given in Eq. (1).

$$\begin{bmatrix} V_a - V_b \\ V_b - V_c \\ 0 \end{bmatrix} = \begin{bmatrix} R_a & -R_b & 0 \\ R_c & R_b + R_c & 0 \\ -R_{fsc} & 0 & R_f + R_{fsc} \end{bmatrix} \begin{bmatrix} i_a \\ i_b \\ i_f \end{bmatrix}$$

$$+ \frac{d}{dt} \begin{bmatrix} L_{aa} - L_{ab} + L_{bc} - L_{ac} & L_{ab} - L_{bb} + L_{bc} - L_{ac} & L_{fa} - L_{fb} \\ L_{ab} - L_{ac} + L_{cc} - L_{bc} & L_{bb} - L_{bc} + L_{cc} - L_{cb} & L_{bf} - L_{cf} \\ L_{fa} - L_{fc} & L_{fb} - L_{fc} & L_{ff} \end{bmatrix} \begin{bmatrix} i_a \\ i_b \\ i_f \end{bmatrix} + \frac{d}{dt} \begin{bmatrix} e_a - e_b \\ e_b - e_c \\ e_f \end{bmatrix} \quad (1)$$

$$T_e = \frac{P}{2} \begin{bmatrix} i_a \\ i_b \\ i_c \\ i_f \end{bmatrix}^T \frac{d}{d\theta} \begin{bmatrix} L_{aa} & L_{ab} & L_{ac} & L_{af} \\ L_{ba} & L_{bb} & L_{bc} & L_{bf} \\ L_{ca} & L_{cb} & L_{cc} & L_{cf} \\ L_{ca} & L_{cb} & L_{cc} & L_{cf} \end{bmatrix} \begin{bmatrix} i_a \\ i_b \\ i_c \\ i_f \end{bmatrix} + P \begin{bmatrix} i_a \\ i_b \\ i_c \\ i_f \end{bmatrix}^T \frac{d}{d\theta} \begin{bmatrix} \lambda_a \\ \lambda_b \\ \lambda_c \\ \lambda_f \end{bmatrix} \quad (2)$$

$$J \frac{d\omega_m}{dt} = T_c - B\omega_m - T_L, \left(\frac{d\theta_m}{dt} = d\omega_m \right) \quad (3)$$

where V is the voltage, R is the resistance, i is the phase current, e is the back electromotive force (EMF), λ is the flux linkage, and subscripts a, b, c, and f are the A, B, C phases and fault phase, respectively. The fault phase is a shorted coil, treated as a single phase in the ITSF of the motor model. The inductance is defined as self-inductance if the subscript is repeated and mutual inductance of the two alphabets if the subscripts are different. For instance, L_{ff} refers to the self-inductance of the phase *fault loop*, and L_{af} is the mutual inductance of phases A and the fault. R_{fsc} is the contact resistance. A detailed physical explanation of the above equation can be found in Ref. [33].

2.3 Inverter and Motor Control Algorithm

The appropriate control algorithm should be implemented and analyzed because the behavior of the short-circuit fault can be affected by the control method [34]. The algorithm includes ITSF of IPMSM modeling based on the electromagnetic data computed using FEM. Fig. 3 shows the inverter–motor control algorithm, which implements a closed-loop field-oriented control (FOC) method with current and speed PI (proportional integral) controllers. IPMSM is controlled by an inverter in the d-q reference frame, as shown in Fig. 3. The parameters of the controllers were auto-tuned using a bandwidth of 30 rad/sec for the speed controller and 318 rad/sec for the current controller. The time step for the simulation was set to 0.5 μs. All these parameters used in this model referred to the parameters of the actual motor and inverter.

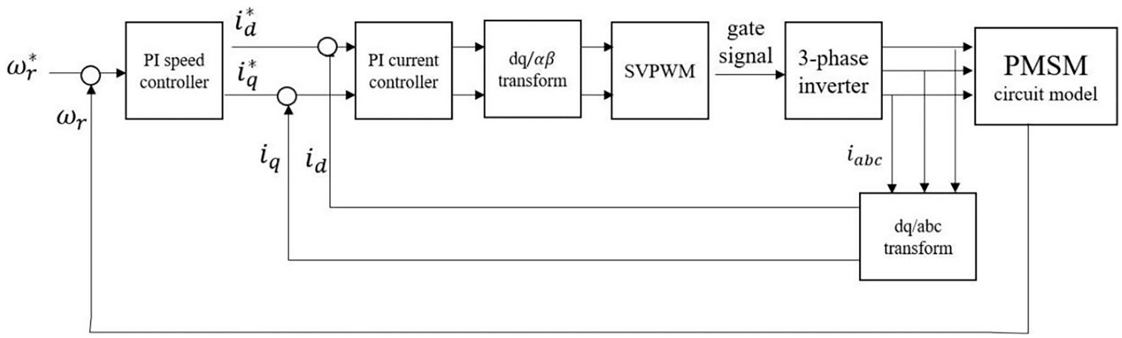

Figure 3: Inverter–motor control diagram for real-time simulation.

2.4 Simulation Results

The phase current (ia, ib, and ic) and short current (if) were simulated using the inverter–motor drive based on the parameters obtained from FEM analysis, as shown in Fig. 4. The time and frequency domains of the healthy and ITSF motors under an operating condition of 3000 rpm and 0.2 N·m were analyzed. The contact resistance is 0.3 Ω. It was observed that a short current can be approximately 2 to 5 times the magnitude of the 3-phase current in the ITSF condition. The short current has an impulse waveform in a single shorted fault because the low inductance single coil could not smooth the pulse width modulation (PWM) waveform voltage applied from the inverter. The short current is maximum in a 26-turn short-circuit fault because the back-EMF producing the short current is proportional to the number of turns of the shorted coil. The short current is an important factor, as heat is produced at the short point in proportion to the square of the short current. The odd harmonic of the motor is larger than that of a healthy motor, and the 3rd and 5th harmonics increase proportionally with the number of shorted turns in 13 and 26 turns short-circuit faults. In particular, the 3rd harmonic can be used as a fault index for diagnosing an ITSF because its value is significantly higher compared to that of the healthy condition. It was observed that the 3rd harmonic of phase current increased by 260% for the 13-turn and 510% for the 26-turn case, compared to the healthy motor. However, the fault signal is not significantly different from that at the healthy condition in a 1-turn shorted, relatively subtle fault condition.

The 3rd harmonic of the back EMF produced by the second inductance and fundamental phase current is not present because it is canceled out in the line by the balanced three phases. However, when a short-circuit fault occurs in one phase, a magnetic flux is generated from the shorted coil in the opposite direction of the main flux, and the flux is distorted and cannot be offset from the 3rd harmonic of the other phase [35]. The fundamental harmonics of the short current and the 3rd harmonic of the phase current under various operation conditions were evaluated under different speeds and loads, as shown in Fig. 5. The short current is proportional to the speed because the flux linkage producing the shorted current increases in proportion to the speed of the motor. Except at 1500 rpm 0.4 N·m condition, the higher the number of shorted turns, the larger the short-circuit current because the flux linkage that produces the shorted current is proportional to the number of turns of the coil. The 3rd harmonic of the phase current, which is used as a fault index, can accurately distinguish the healthy state from the shorted fault for all operation conditions.

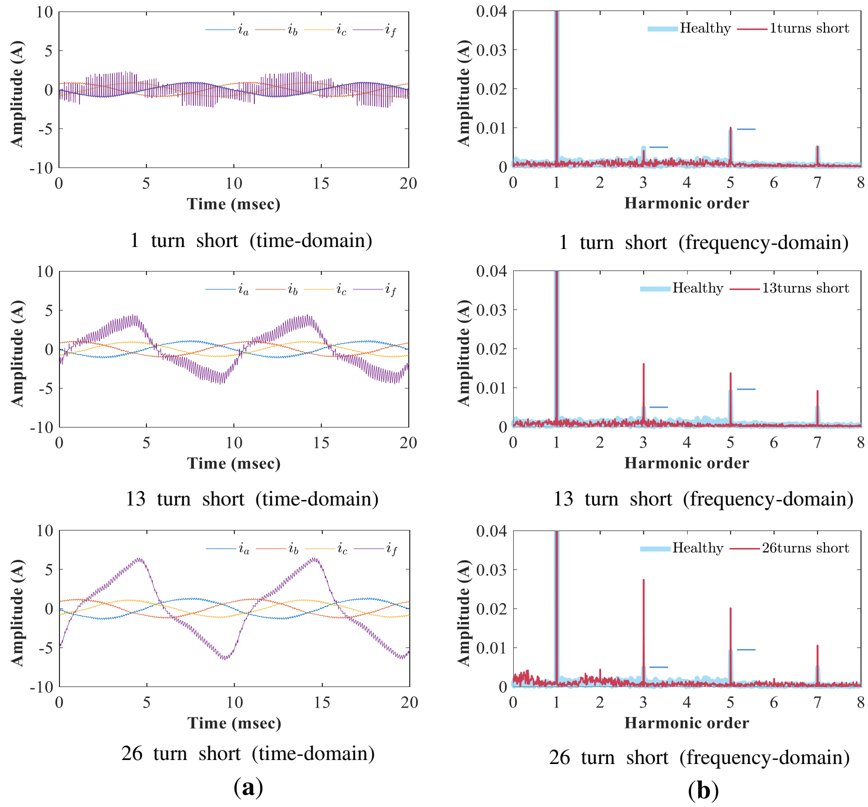

Figure 4: Simulation results for phase and short current at 3000 rpm and 0.2 N·m at various fault conditions: (**a**) time domain (**b**) frequency domain.

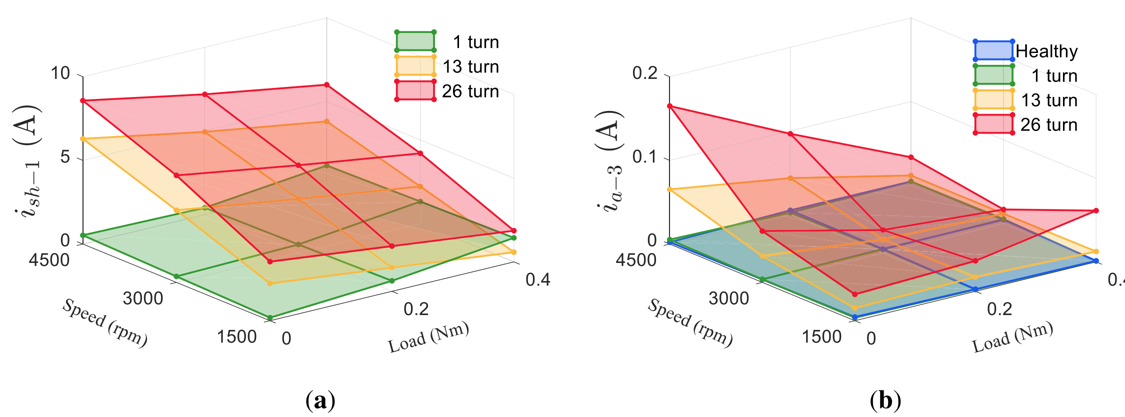

Figure 5: Proposed robust fault indicators from simulation results at various operation conditions for different severity levels: (**a**) first harmonics of short current (**b**) 3rd harmonics of phase current.

3 Experimental Verification

3.1 Experimental Setup

The experiments were carried out to verify the effectiveness of the proposed method for fault diagnosis of ITSF as well as to validate simulation results. Detailed specifications and topology of PSMS used in the experimental study were already provided in the simulation part. The motor was designed using the same specifications as those used in the simulation part. Figs. 6 and 7 show the schematic diagram and photograph of the experimental setup for detecting the ITSF of IPMSM, respectively. Also, Fig. 8 illustrates the implementation of ITSF in this study. To create the ITSF, the insulation of the coil was removed at different turns within a single coil, and additional lead wires were connected to these points and extended externally. These external leads were designed to allow for the adjustment of contact resistance as shown terminal block in Fig. 7. An ITSF was emulated by connecting the neutral point of the stator winding and the number of shorted turns is 1, 13 and 26 as shown in Fig. 6. The insulation resistance of a healthy double-layer enamel wire is a few giga-ohms, but the contact resistance of a shorted wire can decrease to several mili-ohms [36,37]. The contact resistance of the motor was set to 0.3 Ω for safety and equipment protection. Zero contact resistance corresponds to a complete breakdown of the coil's dielectric strength, which may cause hazardous overcurrent during the experiment. Thus, the contact resistance was determined to ensure the short-circuit current does not exceed 15 A. A commercial inverter (V1000, Yasakawa) was used for controlling the IPMSM. The three-phase current and short current were measured using two types of current transformers (CTL-6-S-Z, URD, CTL-24-S28-10Z, URD), respectively. The accelerometer was placed at the center of the motor, and the vibration was monitored using a three-axis piezo accelerometer (3093D7, DYTRAN). The sensor data was acquired using a data acquisition module (NI9223, National Instruments) at 100 kHz and 12.8 kHz for current and vibration data, respectively.

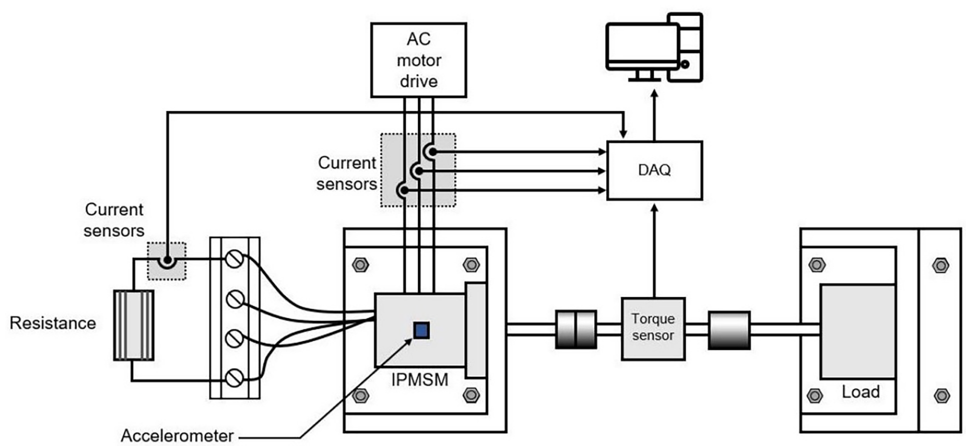

Figure 6: Schematic diagram of the test bed for the experimental validation of ITSF.

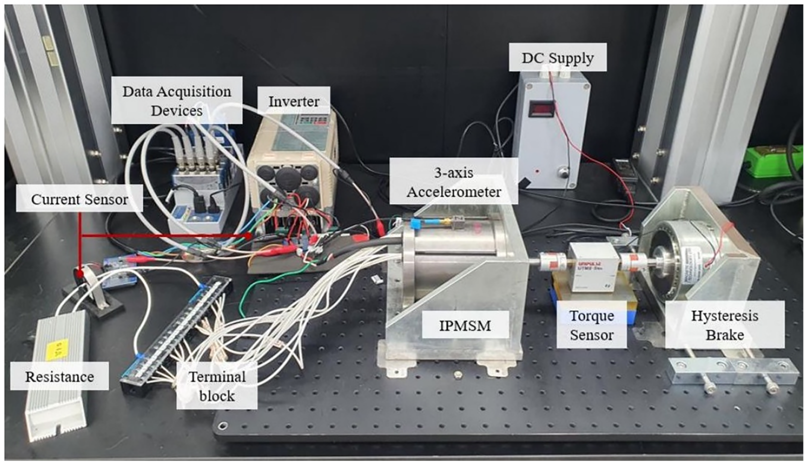

Figure 7: Photograph of the test bed for the ITSF of ITSF.

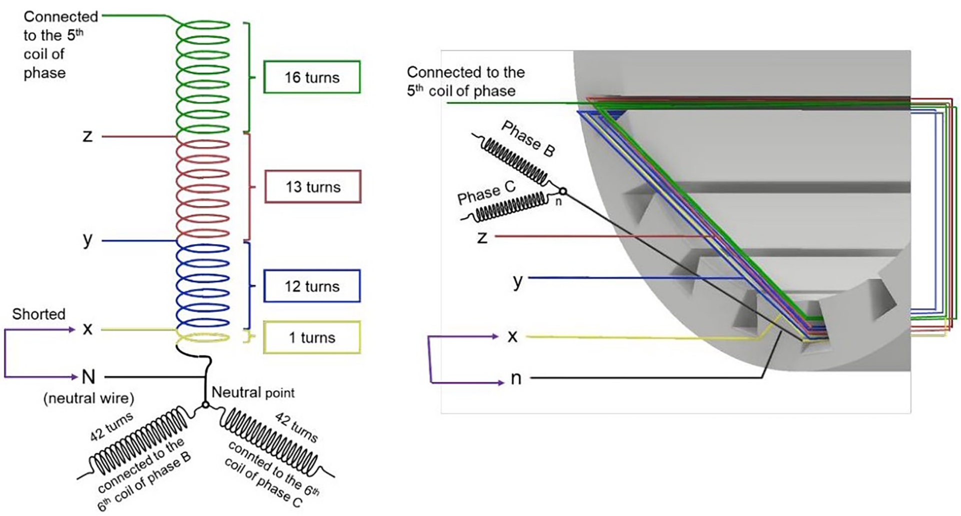

Figure 8: The implementation of the ITSF of the experimental setup in Fig. 7.

3.2 Experimental Results

We investigate the change of phase current, focusing on the odd harmonics in the frequency domain based on results from co-simulation presented in the previous section. The phase currents were monitored, and the experimental and simulation results of the phase currents were compared under different operational conditions, as shown in Fig. 9. In all cases, the amplitude of current through the short circuit of the IPMSM was 4 times higher than the phase current of the healthy motor. The current through the short circuit is dangerously high because a low impedance path can be created in a stator, bypassing the normal load. The current of the phase and short circuit measured in the experimental set-up are similar to those from the simulation results. Hence, in Fig. 10, the 3rd and 5th harmonics increase in both the experimental and simulation results. Furthermore, the difference is most significant at the 3rd harmonic, which is used as a fault detection index. Most of the current harmonics of the simulation results are larger than those from the experiment. Experimental results confirmed that the amplitude of the 3rd harmonic exhibited an error of approximately 15% and 17% compared to the simulation for the healthy motor and the ITSF-faulted motor, respectively. It is estimated that even though the PWM frequency is the same in both results, the inverter dead time was not considered in the simulation.

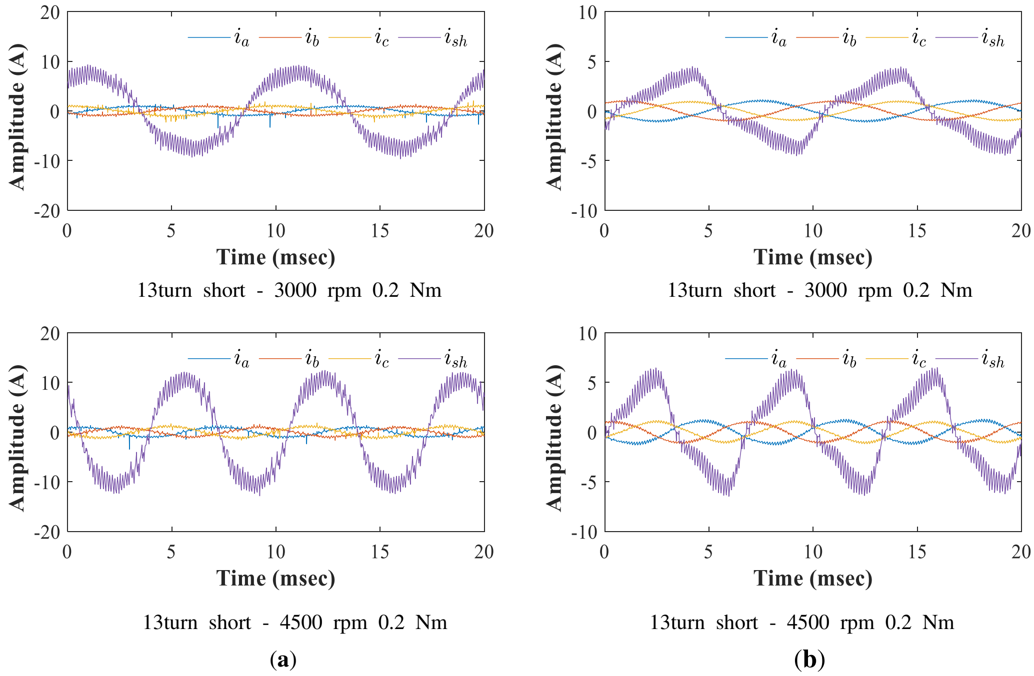

Figure 9: Experimental results for phase and short currents of the 13-turn shorted fault: (**a**) experimental results and (**b**) simulation results.

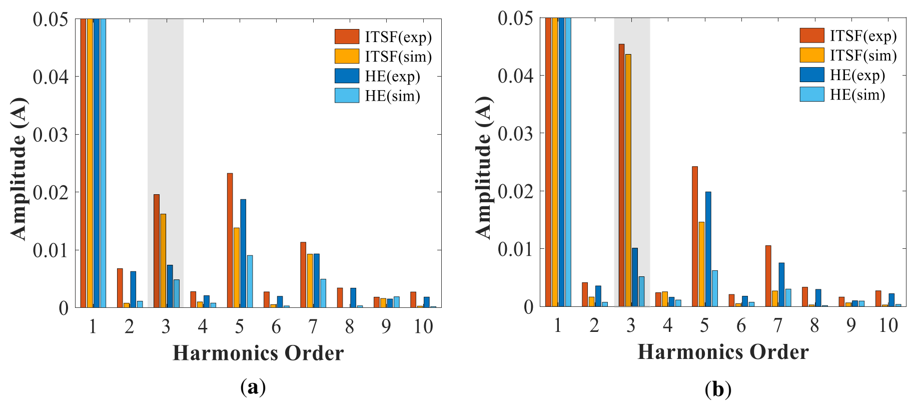

Figure 10: Integer harmonics of the phase current of the healthy and short-circuit fault motor conditions during experiment and simulation: (**a**) 13 turn short, 3000 rpm, 0.2 N·m (**b**) 13 turn short, 4500 rpm, 0.2 N·m.

The first and third harmonics of the phase current of the healthy and short-circuit fault motor conditions during the experiment were investigated, and the results are shown in Fig. 11. In the case of the motor with ITSF, the balanced nature of the three-phase system is distorted, resulting in the third harmonic being changed. However, even when motor torque increases due to applied load, the change in the 3rd harmonic component remains relatively small. These results can be found in Figs. 5b and 11b of our manuscript for both simulation and experiment (as below for experiment). The 3rd harmonic current under ITSF conditions is primarily induced by the distorted Back-EMF within the shorted turns. Since the Back-EMF is directly proportional to the rotor speed variations, it remains largely unaffected by the stator fundamental current used for torque production. As the 3rd harmonic is a zero-sequence component, it is inherently decoupled from the d-q axis currents that govern the electromagnetic torque. This component circulates through the localized fault loop, making it robust against load fluctuations while serving as a reliable indicator of fault severity at a given speed. The 3rd harmonic of phase current can detect 13, 26 shorted faults from the healthy condition under all operating conditions. However, the 3rd harmonics of a 1-turn shorted fault cannot be clearly distinguished from the healthy condition. Analytical and experimental results confirm that an ITSF severity of 13 turns with a contact resistance of 0.3 Ω is reliably diagnosable across all operating conditions. This condition causes a motor efficiency drop of 3.1%, and it enables early-stage diagnosis of the ITSF. In addition, the signal from the vibration sensor, which has been widely used in condition monitoring for PMSM, shows that there is no significant difference in the vibration of 1 and 13 turns shorted and healthy states under all operating conditions. As depicted in Fig. 12, it is expected that it is difficult to diagnose ITSF with low severity (1 and 13 turns). It means that the vibration signals alone are not enough to make a solid diagnosis of ITSF. It is possibly because the vibration from flux linkage distortion due to 1 shorted coil is smaller than other vibrations due to mechanical factors. In contrast, under the condition of 4500 rpm, the vibration of the 13-turn shorted motor was 13%–25% larger than that of the healthy motor, depending on the load torque, whereas that of the 26-turn shorted fault motor was 1.5–4 times larger than that of the healthy motor. Therefore, except for 1 and 13 turn shorted faults, the RMS value of the vibration can be one of the fault indicators for ITSF under all operational conditions, which is similar to the diagnosis performance of the current sensor. Therefore, this study demonstrates that current sensor-based diagnosis is more advantageous than vibration-based diagnosis for detecting ITSF in PMSM.

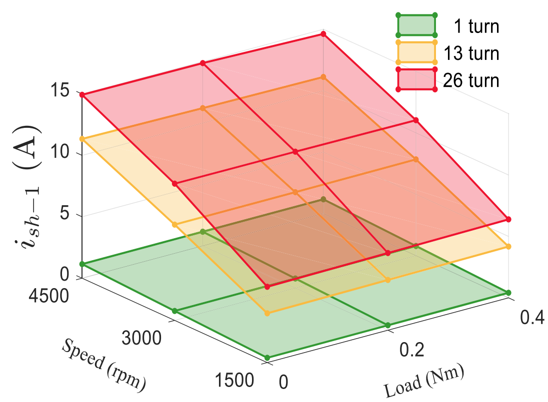

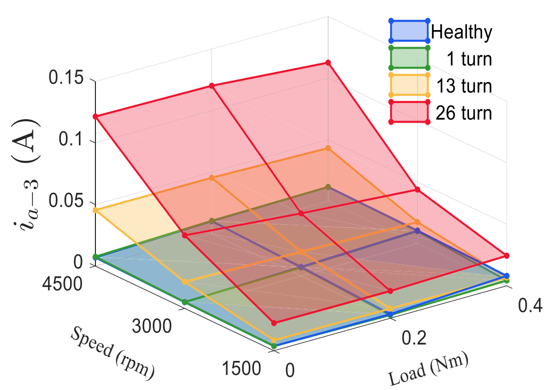

Figure 11: Proposed robust fault indicators from experimental results at various operation conditions for different severity levels: (**a**) first harmonics of short current (**b**) 3rd harmonics of phase current.

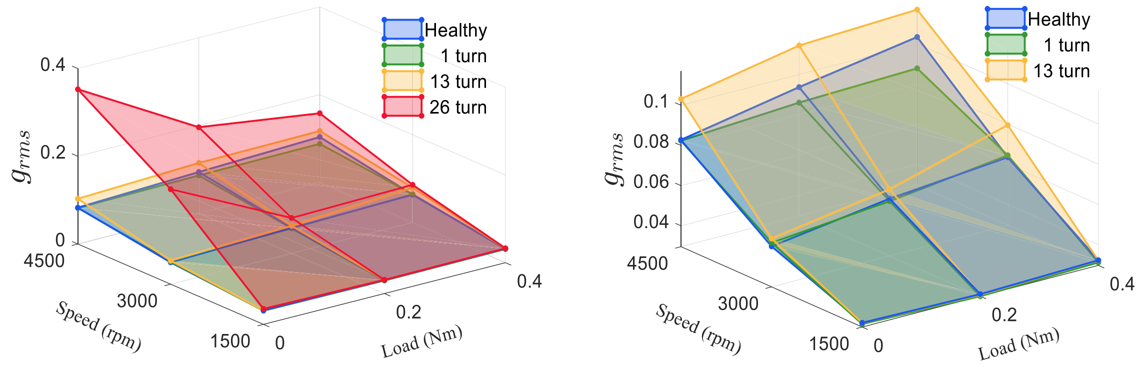

Figure 12: RMS value of vibration as a function of fault severity and driving conditions under various operating conditions: (**a**) healthy, 1, 13, 26 turn shorted fault (**b**) healthy, 1, 13 turn shorted fault.

4 Conclusion

This study investigated the characteristics and diagnostic methods for inter-turn short-circuit faults (ITSF) in an interior permanent magnet synchronous motor (IPMSM) operating under various speeds and loads. To monitor the essential data for ITSF diagnosis and identify fault indicators through signal processing, a co-simulation framework based on a digital twin approach was employed. A 2D finite element analysis (FEA) of the ITSF in the IPMSM was conducted to evaluate the electromagnetic effects. The inverter and motor were co-simulated in real time by implementing a closed-loop field-oriented control (FOC) algorithm derived from the FEA results. A fault diagnosis technique was then applied using the phase current data obtained from the co-simulation, and the method was verified with experimental results.

The simulation results show that the magnetic flux of a healthy coil is distorted by a shorted coil, owing to the flux generated in the opposite direction to the main flux. It was confirmed that the third harmonic of the phase current, resulting from this magnetic distortion, can serve as a fault indicator. It was also found that higher motor speeds and a greater number of shorted turns lead to a stronger fault signal.

Although a stronger fault indicator at higher speeds can be advantageous, this characteristic inherently limits the proposed algorithm to fixed-speed operation. However, because operational systems typically monitor speed, acquiring and analyzing current data at a designated speed does not pose a significant issue for ITSF diagnosis. Based on both simulation and experimental results, 13-turn and 26-turn short-circuit faults were accurately distinguished from the healthy state under all operating conditions.

Furthermore, vibration analysis of short-circuit faults using an accelerometer yielded similar results, although its sensitivity for fault detection was slightly lower than that of phase current spectral analysis under certain conditions. Therefore, this study confirms that ITSF diagnosis in PMSMs is feasible using low-cost, built-in current sensors instead of expensive vibration sensors, which are already implemented in most traction systems.

Acknowledgement: This work was supported by Konkuk University in 2023.

Funding Statement: The authors received no specific funding for this study.

Author Contributions: The authors confirm contribution to the paper as follows: Conceptualization, Junho Lee and Namsu Kim; methodology, Junho Lee; software, Sanghyun Park; validation, Younghun Lee; formal analysis, Junho Lee; investigation, Junho Lee; resources, Namsu Kim; data curation, Sanghyun Park; writing—original draft preparation, Junho Lee; writing—review and editing, Namsu Kim; visualization, Younghun Lee; supervision, Namsu Kim; project administration, Namsu Kim; funding acquisition, Namsu Kim. All authors reviewed and approved the final version of the manuscript.

Availability of Data and Materials: Data available on request from the authors.

Ethics Approval: Not Applicable.

Conflicts of Interest: The authors declare no conflicts of interest.

Abbreviations

The following abbreviations are used in this manuscript

FEM	Finite element method
EVs	Electric vehicles
IPMSM	Interior permanent magnet synchronous motor
PHM	Prognostic and health management
ITSF	Interturn short-circuit fault
WBG	Wide band gap
SiC	Silicon carbide
MCSA	Motor current signature analysis
FFT	Fast Fourier transform
STFT	Short-time Fourier transform
EMF	Electromotive force
LUT	Look-up table

References

1. Liu Z, Jia Z, Vong CM, Han J, Yan C, Pecht M. A patent analysis of prognostics and health management (PHM) innovations for electrical systems. IEEE Access. 2018;6:18088–107. doi:10.1109/ACCESS.2018.2818114.
2. Aghabali I, Bauman J, Kollmeyer PJ, Wang Y, Bilgin B, Emadi A. 800-V electric vehicle powertrains: review and analysis of benefits, challenges, and future trends. IEEE Trans Transp Electrif. 2021;7(3):927–48. doi:10.1109/TTE.2020.3044938.
3. Moghadam DE, Herold C, Zbinden R. Electrical insulation at 800 V electric vehicles. In: Proceedings of the 2020 International Symposium on Electrical Insulating Materials (ISEIM); 2020 Sep 13–17; Tokyo, Japan. p. 115–9.
4. Allca-Pekarovic A, Kollmeyer PJ, Mahvelatishamsabadi P, Mirfakhrai T, Naghshtabrizi P, Emadi A. Comparison of IGBT and SiC inverter loss for 400 V and 800 V DC bus electric vehicle drivetrains. In: Proceedings of the 2020 IEEE Energy Conversion Congress and Exposition (ECCE); 2020 Oct 11–15; Detroit, MI, USA. p. 6338–44. doi:10.1109/ecce44975.2020.9236202.
5. Bubert A, Oberdieck K, Xu H, De Doncker RW. Experimental validation of design concepts for future EV-traction inverters. In: Proceedings of the 2018 IEEE Transportation Electrification Conference and Expo (ITEC); 2018 Jun 13–15; Long Beach, CA, USA. p. 795–802. doi:10.1109/ITEC.2018.8450253.
6. Jung C. Power up with 800-V systems: the benefits of upgrading voltage power for battery-electric passenger vehicles. IEEE Electrif Mag. 2017;5(1):53–8. doi:10.1109/MELE.2016.2644560.
7. Anderson P. The electric vehicle industry will shift to advanced 800-volt architectures. 2022 [cited 2026 May 1]. Available from: https://www.carscoops.com.
8. Kaufhold M, Borner G, Eberhardt M, Speck J. Failure mechanism of the interturn insulation of low voltage electric machines fed by pulse-controlled inverters. IEEE Electr Insul Mag. 1996;12(5):9–16. doi:10.1109/57.537190.
9. Dehlinger N, Stone G. Surface partial discharge in hydrogenerator *Stator* windings: causes, symptoms, and remedies. IEEE Electr Insul Mag. 2020;36(3):7–18. doi:10.1109/MEI.2020.9063559.

10. Lee K, Fereydoonian M, Benson M, Lee W. Partial discharge and electromagnetic interference under repetitive voltage pulses with high slew rate in AC machine drives. In: Proceedings of the 2022 IEEE/AIAA Transportation Electrification Conference and Electric Aircraft Technologies Symposium (ITEC+EATS); 2022 Jun 15–17; Anaheim, CA, USA. p. 917–22. doi:10.1109/ITEC53557.2022.9814013.
11. He J, Somogyi C, Strandt A, Demerdash NAO. Diagnosis of stator winding short-circuit faults in an interior permanent magnet synchronous machine. In: Proceedings of the 2014 IEEE Energy Conversion Congress and Exposition (ECCE); 2014 Sep 14–18; Pittsburgh, PA, USA. p. 3125–30. doi:10.1109/ECCE.2014.6953825.
12. Ebrahimi BM, Faiz J. Feature extraction for short-circuit fault detection in permanent-magnet synchronous motors using stator-current monitoring. IEEE Trans Power Electron. 2010;25(10):2673–82. doi:10.1109/TPEL.2010.2050496.
13. Strangas EG, Aviyente S, Zaidi SSH. Time-frequency analysis for efficient fault diagnosis and failure prognosis for interior permanent-magnet AC motors. IEEE Trans Ind Electron. 2008;55(12):4191–9. doi:10.1109/TIE.2008.2007529.
14. Gurusamy V, Bostanci E, Li C, Qi Y, Akin B. A stray magnetic flux-based robust diagnosis method for detection and location of interturn short circuit fault in PMSM. IEEE Trans Instrum Meas. 2021;70:3500811–11. doi:10.1109/TIM.2020.3013128.
15. Hou M, Shi H. Stator-winding incipient shorted-turn fault detection for motor system in motorized spindle using modified interval observers. IEEE Trans Instrum Meas. 2021;70:3505716–16. doi:10.1109/TIM.2020.3040994.
16. Urresty JC, Riba JR, Romeral L. Application of the zero-sequence voltage component to detect stator winding inter-turn faults in PMSMs. Electr Power Syst Res. 2012;89(11):38–44. doi:10.1016/j.epsr.2012.02.012.
17. Sarikhani A, Mohammed OA. Inter-turn fault detection in PM synchronous machines by physics-based back electromotive force estimation. IEEE Trans Ind Electron. 2013;60(8):3472–84. doi:10.1109/TIE.2012.2222857.
18. Qi Y, Bostanci E, Zafarani M, Akin B. Severity estimation of interturn short circuit fault for PMSM. IEEE Trans Ind Electron. 2019;66(9):7260–9. doi:10.1109/TIE.2018.2879281.
19. Baruti KH, Gurusamy V, Erturk F, Akin B. A robust and practical approach to estimate the number of shorted turns in PMSM with ITSC faults. IEEE J Emerg Sel Top Power Electron. 2021;9(3):2839–49. doi:10.1109/JESTPE.2020.3011692.
20. Niu G, Dong X, Chen Y. Motor fault diagnostics based on current signatures: a review. IEEE Trans Instrum Meas. 2023;72:3520919–19. doi:10.1109/TIM.2023.3285999.
21. Zhao Z, Fan F, Wang W, Liu Y, See KY. Detection of stator interturn short-circuit faults in inverter-fed induction motors by online common-mode impedance monitoring. IEEE Trans Instrum Meas. 2021;70:3513110–10. doi:10.1109/TIM.2021.3066193.
22. Sun Z, Wang J, Howe D, Jewell G. Analytical prediction of the short-circuit current in fault-tolerant permanent-magnet machines. IEEE Trans Ind Electron. 2008;55(12):4210–7. doi:10.1109/TIE.2008.2005019.
23. Arumugam P, Hamiti T, Gerada C. Modeling of different winding configurations for fault-tolerant permanent magnet machines to restrain interturn short-circuit current. IEEE Trans Energy Convers. 2012;27(2):351–61. doi:10.1109/TEC.2012.2188138.
24. Jiang Y, Zhang Z, Jiang W, Geng W, Huang J. Three-phase current injection method for mitigating turn-to-turn short-circuit fault in concentrated-winding permanent magnet aircraft starter generator. IET Electr Power Appl. 2018;12(4):566–74. doi:10.1049/iet-epa.2017.0754.
25. Zhao J, Guan X, Li C, Mou Q, Chen Z. Comprehensive evaluation of inter-turn short circuit faults in PMSM used for electric vehicles. IEEE Trans Intell Transp Syst. 2021;22(1):611–21. doi:10.1109/TITS.2020.2987637.
26. Qi Y, Bostanci E, Gurusamy V, Akin B. A comprehensive analysis of short-circuit current behavior in PMSM interturn short-circuit faults. IEEE Trans Power Electron. 2018;33(12):10784–93. doi:10.1109/TPEL.2018.2809668.
27. Ullah Z, Hur J. Analysis of inter-turn-short fault in an FSCW IPM type brushless motor considering effect of control drive. IEEE Trans Ind Appl. 2020;56(2):1356–67. doi:10.1109/TIA.2019.2961878.
28. Ko Y, Lee Y, Oh J, Park J, Chang H, Kim N. Current signature identification and analysis for demagnetization fault diagnosis of permanent magnet synchronous motors. Mech Syst Signal Process. 2024;214(11):111377. doi:10.1016/j.ymssp.2024.111377.

29. Jin L, Mao Y, Wang X, Lu L, Zhu J. Fault diagnosis of PMSM drives based on digital twin modeling. In: Proceedings of the 2024 IEEE 10th International Power Electronics and Motion Control Conference (IPEMC2024-ECCE Asia); 2024 May 17–20; Chengdu, China. p. 422–5. doi:10.1109/IPEMC-ECCEAsia60879.2024.10567575.
30. Yu S, Wang M, Pang S, Song L, Zhai X, Zhao Y. TDMSAE: a transferable decoupling multi-scale autoencoder for mechanical fault diagnosis. Mech Syst Signal Process. 2023;185(9):109789. doi:10.1016/j.ymssp.2022.109789.
31. Li Y, Zhou J, Geng H, Du T, Zhang J, Lv H. A coupling simulation of converter field circuit for permanent magnet synchronous motor based on simplorer and Maxwell. In: Proceedings of the 2018 IEEE International Conference on Mechatronics and Automation (ICMA); 2018 Aug 5–8; Changchun, China. p. 1475–80. doi:10.1109/ICMA.2018.8484730.
32. Ullah Z, Kim KT, Park JK, Hur J. Comparative analysis of scalar and vector control drives of IPMSM under interturn fault condition considering nonlinearities. In: Proceedings of the 2015 IEEE Energy Conversion Congress and Exposition (ECCE); 2015 Sep 20–24; Montreal, QC, Canada. p. 366–72. doi:10.1109/ECCE.2015.7309711.
33. Mohammed OA, Liu S, Liu Z. Physical modeling of PM synchronous motors for integrated coupling with machine drives. IEEE Trans Magn. 2005;41(5):1628–31. doi:10.1109/TMAG.2005.846122.
34. Zafarani M, Bostanci E, Qi Y, Goktas T, Akin B. Interturn short-circuit faults in permanent magnet synchronous machines: an extended review and comprehensive analysis. IEEE J Emerg Sel Top Power Electron. 2018;6(4):2173–91. doi:10.1109/JESTPE.2018.2811538.
35. Gu BG. Study of IPMSM interturn faults part I: development and analysis of models with series and parallel winding connections. IEEE Trans Power Electron. 2016;31(8):5931–43. doi:10.1109/TPEL.2015.2496142.
36. Turabee G, Cosma G, Madonna V, Giangrande P, Khowja MR, Vakil G, et al. Predicting insulation resistance of enamelled wire using neural network and curve fit methods under thermal aging. In: Proceedings of the 2020 International Joint Conference on Neural Networks (IJCNN); 2020 Jul 19–24; Glasgow, UK. p. 1–7. doi:10.1109/IJCNN48605.2020.9207378.
37. Andruşcă M, Adam M, Burlica R, Munteanu A, Dragomir A. Considerations regarding the influence of contact resistance on the contacts of low voltage electrical equipment. In: Proceedings of the 2016 International Conference and Exposition on Electrical and Power Engineering (EPE); 2016 Oct 20–22; Iasi, Romania. p. 123–8. doi:10.1109/ICEPE.2016.7781317.